Elucidating the formation of Al–NBO bonds, Al–O–Al linkages and clusters in alkaline-earth aluminosilicate glasses based on molecular dynamics simulations

Sudheer Ganisetti, Anuraag Gaddam, Rajesh Kumar, Sathravada Balaji, Glenn Mather, Maria Pascual, Margit Fabian, Renée Siegel, Jürgen Senker, Vladislav Kharton, et al.

Elucidating the formation of Al–NBO bonds, Al–O–Al linkages and clusters in alkaline-earth aluminosilicate glasses based on molecular dynamics simulations†

Sudheer Ganisetti,[a] Anuraag Gaddam,[b] Rajesh Kumar,[c] Sathravada Balaji,[d] Glenn C. Mather,[e] Maria J. Pascual,[e] Margit Fabian,[f] Renée Siegel,[g] Jürgen Senker,[g] Vladislav V. Kharton,[h] Julien Guénolé,[i] N. M. Anoop Krishnan,*[d] José M. F. Ferreira*[c] and Amarnath R. Allu*[d]

Exploring the reasons for the initiation of Al–O–Al bond formation in alkali-earth alumino silicate glasses is a key topic in the glass-science community. Evidence for the formation of Al–O–Al and Al–NBO bonds in the glass composition 38.7CaO–9.7MgO–12.9Al_2O_3–38.7SiO_2 (CMAS, mol%) has been provided based on Molecular Dynamics (MD) simulations. Analyses in the short-range order confirm that silicon and the majority of aluminium cations form regular tetrahedra. Well-separated homonuclear (Si–O–Si) and heteronuclear (Si–O–Al) cluster regions have been identified. In addition, a channel region (C-Region), separated from the network region, enriched with both NBO and non-framework modifier cations, has also been identified. These findings are in support of the previously proposed extended modified random network (EMRN) model for aluminosilicate glasses. A detailed analysis of the structural distributions revealed that a majority of Al, 51.6%, is found in Si–O–Al links. Although the formation of Al–O–Al and Al–NBO bonds is energetically less favourable, a significant amount of Al is found in Al–O–Al links (33.5%), violating Lowenstein's rule, and the remainder is bonded with non-bridging oxygen (NBO) in the form of Al–NBO (Al–O–(Ca, Mg)). The conditions necessary for the formation of less favourable bonds are attributed to the presence of a high amount of modifier cations in current CMAS glass and their preferable coordination.

[a] *Department of Materials Science and Engineering, Institute I, Friedrich-Alexander-Universität Erlangen-Nürnberg, Martensstr. 5, 91058 Erlangen, Germany*
[b] *Department of Materials and Ceramic Engineering, CICECO, University of Aveiro, 3810–193 Aveiro, Portugal*
[c] *Department of Civil Engineering, Indian Institute of Technology Delhi, Hauz Khas, New Delhi, India 110016. E-mail: jmf@ua.pt; Fax: +351-234-370204; Tel: +351-234-370242*
[d] *Glass Division, CSIR-Central Glass and Ceramic Research Institute, 700032, Kolkata, India. E-mail: aareddy@cgcri.res.in, krishnan@iitd.ac.in; Fax: +91-33-24730957; Tel: +91-33-23223421, +91-11-26591223*
[e] *Instituto de Cerámica y Vidrio (CSIC), C/Kelsen 5, Campus de Cantoblanco, 28049 Madrid, Spain*
[f] *Centre for Energy Research, Hungarian Academy of Sciences, 1121 Budapest Konkoly-Thegest. 29-33, Hungary*
[g] *Inorganic Chemistry III, University of Bayreuth, 95440 Bayreuth, Germany*
[h] *Institute of Solid State Physics RAS, 142432 Chernogolovka, Moscow District, Russia*
[i] *Institute of Physical Metallurgy and Materials Physics, RWTH Aachen University, 52056 Aachen, Germany*

† Electronic supplementary information (ESI) available: The influence of various parameters (potential, size, cooling rate and cooling method) on the distribution of framework cations. See DOI: 10.1039/c9cp04332b

1. Introduction

Alkaline-earth aluminosilicate glasses are promising materials for high-power laser applications,[1] for solid oxide fuel cells as sealing materials[2] and for long-term immobilization of complex mixed radioactive wastes.[3] Understanding the composition–structure–property relationship in aluminosilicate oxide glasses has been the main driving force behind the rapid development of glass-based materials for these applications.[1–8] The non-crystalline structure of aluminosilicate glasses strongly depends on the skeletal network consisting of the framework tetrahedron (Si and Al) units present in it.[9] The compensated continuous random network (CCRN) model and the modified random network (MRN) structural model are widely used models for explaining the distribution of framework units in aluminosilicate glasses.[5,10,11] Both models obey the well-known Al-avoidance principle or Lowenstein's rule.[12] This rule states that: (i) Al–O–Al bonds are energetically less favourable and are avoided over Si or other atoms such as P, and (ii) in the case of formation of Al–O–Al bonds, at least one of the Al atoms should have a coordination

number greater than four. Experimentally, this rule is valid for many different silicate glass compositions with moderate alumina doping.[13–15] However, it has been reported that Al–O–Al bonds are more prominent in magnesium aluminosilicate glasses than in calcium- or sodium-containing aluminosilicate glasses.[16–20] This outcome questions the validity of the Al-avoidance principle and thereby limits the applicability of the MRN and CCRN models for aluminosilicate glasses. New alternative or extended models are, therefore, essential for explaining the distribution of AlO_4 and SiO_4 tetrahedral units, as well as the formation of Al–O–Al bonds, in alkaline-earth aluminosilicate glasses.

Many studies have reported the presence of Al–O–Al bonds in alkali/alkaline-earth/rare-earth aluminosilicate glasses.[21–23] Magic-angle spinning (MAS)-nuclear magnetic resonance (NMR) spectroscopy of ^{29}Si and ^{17}O nuclei and molecular dynamics (MD) simulations have been employed in many studies to quantify the distribution of various $Q^n(m\mathrm{Al})$ units in aluminosilicate glasses and identify the existence of Al–O–Al units.[6,22–27] Nevertheless, the presence of Al–O–Al bonds in non-crystalline structures has mostly been justified based on their chemical composition. For example, for a constant mole fraction of silica in alkali/alkaline-earth aluminosilicate glasses, the fraction of Al–O–Al and Si–O–Al bonds increases with increasing polymerization as alkali/alkaline-earth species are replaced with Al_2O_3.[24,28] Furthermore, it is also concluded that increasing the alkali/alkaline-earth-cation field strength increases the population of Al–O–Al sites.[29,30] Owing to their highly efficient charge-compensation capability, trivalent rare-earth cations stabilize Al–O–Al configurations and increase the fraction of Al–O–Al bonds in aluminosilicate glasses.[31,32] Very recently, we have studied the alkaline-earth aluminosilicate glass system for its application as a sealing material for solid oxide fuel cells.[2] Detailed analysis of the deconvoluted ^{29}Si MAS-NMR spectra revealed that 60% of Al participates in Al–O–Al bonds and that 40% of Al exists in Al–O–Si bonds.[33] Nevertheless, in addition to the effective influence of alkaline-earth-cation field strength, MD simulations are also essential for interpreting the experimental results and to explore the origin of the formation of Al–O–Al bonds.

Furthermore, due to limited direct experimental accessibility, the estimation of Al in Al–O–Al linkages is largely dependent on the selection of the structural model. ^{17}O NMR may be used for direct quantitative measurement,[34–36] but is inaccessible to most glass researchers due to its expense. A good structural model is, therefore, necessary for accurate estimation of Al in Al–O–Al linkages. In the $43.1CaO–12.5Al_2O_3–44.4SiO_2$ (mol%, CAS) glass composition,[22] the random-intermediate range order (R–IRO) model estimates the quantity of Al in Al–O–Al units to be 58%, while the Quasi-Heterogeneous Intermediate Range Order (QH–IRO) model predicts a much lower value of 17%. A more appropriate structural model is, therefore, required in order to identify the distribution of framework units and to explain the formation of Al–O–Al bonds. In this context, we recently proposed an extended modified random network (EMRN) model to explain the formation of Al–O–Al bonds in aluminosilicate glasses.[33] Note that our previous work[33] uses the name ''new modified random network'', which is inaccurate as only some exclusive extensions are made to the base MRN model. According to the EMRN model, which evolves from the MRN model,[5] the framework units in aluminosilicate glasses form a network-structure region combining clusters of heteronuclear units and homonuclear units, as shown in Fig. 5 of ref. 33. The as-formed heteronuclear, homonuclear and R-cluster regions are connected with each other. Here, we evidence the essential formation of clusters of heteronuclear and homonuclear units in aluminosilicate glasses.

In the present study, the previously reported calcium magnesium aluminosilicate (CMAS) glass composition[2] (mol%) $38.7CaO–9.7MgO–12.9\ Al_2O_3–38.7\ SiO_2$ is selected for assessing the distribution of the framework units in the network structure region by using MD simulations. Furthermore, the origin for the formation of Al–O–Al bonds in CMAS glass is evidenced.

2. Method and models

2.1 Molecular dynamics simulation method

Molecular dynamics (MD) simulations are performed using the LAMMPS code.[37] The atomic interactions are computed using two different interatomic potentials designed by Miyake *et al.*[38] and Pedone *et al.*[39] Hereafter, the glass samples prepared with the Miyake and Pedone potentials are termed as Miyake glass (M-glass) and Pedone glass (P-glass), respectively (Table 1). The Miyake potential consists of a short-range repulsive term, a van der Waals attractive term, a Morse two-body term and a long-range Coulombic term. The Pedone potential consists of a short-range repulsive term, which is different from that used by Miyake, a Morse two-body term and a long-range Coulombic term. In order to check the reliability of the potential, some test cases were performed where the structural properties obtained from the simulations were compared with the available experimental data; these results are presented in the ESI.† In both potentials, the Coulombic interactions are computed by using Ewald summation[40] with a relative precision of 10^{-6} in force by limiting the real-space calculations within a cut-off radius of 12 Å. Periodic boundary conditions are imposed along all the three axes to imitate a bulk sample, thus preventing any surface effect. The Velocity Verlet algorithm with a time step of 1 fs is used to integrate the Newton's equations of motion. Nose–Hoover thermostat and barostats are used to control the temperature and pressure, when required.[41,42]

Table 1 Sample names and key parameters used for the preparation of glass and resultant cation–oxygen distances at 300 K

Sample name	Potential	Total atoms	Cooling rate (K ps^{-1})	Density (g cm^{-3})	Si–O (Å)	Al–O (Å)	Ca–O (Å)	Mg–O (Å)
M-Glass	Miyake	2774	10	2.75	1.62	1.76	2.42	2.11
P-Glass	Pedone	2774	10	2.94	1.59	1.73	2.32	2.04

2.2 Sample preparation

The calcium magnesium aluminosilicate (CMAS) glass composition employed in the present study is 38.7CaO–9.7MgO–12.9Al_2O_3–38.7SiO_2 (mol%).[2,33] First, n number (n = 280, 553, 1393, 2774 and 11 096) of atomic positions are generated randomly in a cubic box. The box dimensions are set to reproduce the experimental density at room temperature.[33] The atom types are then assigned randomly according to the composition. While generating the atomic positions, we ensured that we had inter atomic distances larger than 1.8 Å to avoid any artificial high-energy, short-range interactions. The ion position of the initial sample is relaxed by molecular statics when using the conjugate gradient method. This sample is then thermalized for 10 ps at 300 K within the micro-canonical ensemble (*NVE*) before ramping the temperature from 300 K to 5000 K with a heating rate of 100 K ps^{-1} within the canonical ensemble (*NVT*). After heating to 5000 K, the melt is equilibrated for about 100 ps using the *NVT* ensemble to avoid any possible formation of artificial clusters. The melt is then quenched down to 300 K with several cooling rates, ranging from 0.1 to 100 K ps^{-1} [43] using the *NVT* ensemble. At 300 K, the samples are thermalized for about 200 ps using an isobaric-isothermal ensemble (*NPT*) to remove thermomechanical stresses accumulated during the quenching procedure. The final stress-free samples are collected at room temperature to investigate various structural properties, including pair-distribution function and neutron scattering structure factor. To improve the statistical relavance of our analysis, five samples for each potential with different initial structures are prepared. The visualisation of atomic structures and the construction of surface meshes are performed using the visualisation software OVITO.[44] The neutron scattering structure factor of the modeled glass is computed using the ISAACS structural analysis tool.[45]

3. Results

The sample names along with the parameters used during the preparation, and some of their physical and structural properties computed at room temperature, are presented in Table 1. The results of a sample containing 2774 atoms quenched with 10 K ps^{-1} using the Pedone potential are discussed unless otherwise specified. The Miyake potential leads to a room temperature density of 2.75 g cm^{-3} (Table 1), slightly lower (5.5%) than the experimental density (2.91 g cm^{-3}). The Pedone potential estimates a density of 2.94 g cm^{-3}, closer to the experimental value.

3.1 Bond lengths and coordination number

In Fig. 1a, the total structure factors $S(Q)$ of P-glass and M-glass from the MD simulations are compared with the experimentally obtained neutron-diffraction $S(Q)$ within a range of 0.45–10.0 $Å^{-1}$.[2,46] The appearance of broad lines confirms the structural disorder of the simulated CMAS glass. Fig. 1b shows a comparison of the partial pair distribution function (PPDF) of oxygen atoms with each cation for P-glass and M-glass, in solid and dashed lines, respectively. The position of the first peak maxima of each PPDF curve is considered as the bond length, *i.e.*, the mean distance between the corresponding cation and its first-neighbour oxygen, and these are presented in Table 1. The bond lengths of Si–O, Al–O, Ca–O and Mg–O are shorter in the P-glass than the corresponding bond lengths in the M-glass, in accordance with the higher density of M-glass. Nevertheless, except for Mg–O, the obtained bond lengths of the cations in the M and P glasses compare well with the previously reported values.[33] The PPDF curves of Si and Al show a clear separation between the first and second O neighbours. Hence, we considered a cut-off radius of 2.5 Å to determine the neighbouring O atoms in the first coordination shell. Conversely, the PPDF curves of Ca and Mg show no clear separation between the first and second O neighbours. However, 3.10 Å and 2.75 Å were found to be good approximations for the first minima, respectively. These values were, thus, chosen to be the cut-off radii to determine the neighbouring O in the first coordination shell for M-glass. For the P-glass sample, 3.0 and 2.5 Å were chosen to be the cut-off radii for the Ca–O and Mg–O atom pairs, respectively. The yielded mean coordination numbers of Si, Al, Ca and Mg for M-glass are 4.00,

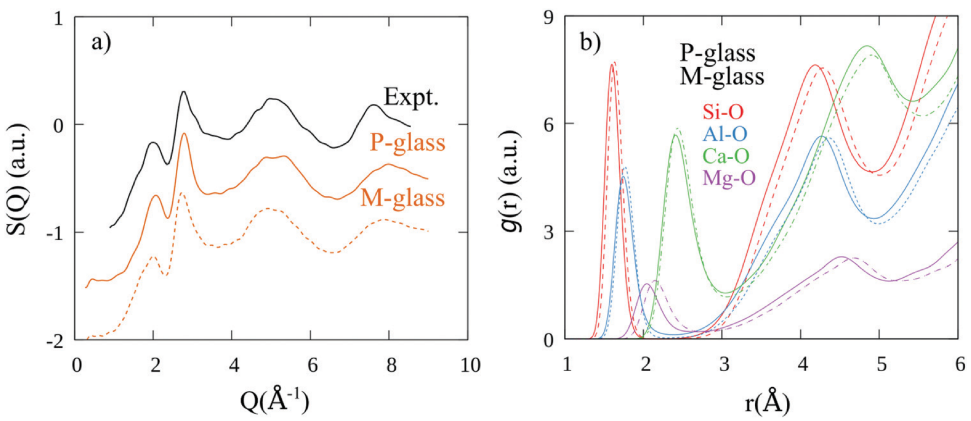

Fig. 1 (a) Comparison of the experimental values of the neutron-structure factor with those obtained from MD simulations and (b) comparison of partial pair distribution function over interparticle distance of cation–oxygen for CMAS glass prepared with Miyake (dashed lines) and Pedone (solid lines) potentials.

4.05, 6.59 and 5.04, respectively, whilst 4.00, 4.13, 6.20 and 4.60, respectively, are obtained for P-glass. The obtained mean coordination numbers for Si and Al atoms from MD simulations correlate well with the values reported in a previous article, which were calculated by Reverse Monte Carlo (RMC) simulations.[2] Since the results are consistent for both M- and P-glasses, in this work we present the results for the P-glass, unless specified otherwise.

3.2 Distribution of SiO_4 and AlO_4 structural units

To identify the distribution of tetrahedra, we used the notation $Q^n_T(mT')$ with $0 \le m \le n \le 4$ and $T \neq T'$.[26,47] T and T′ represent types of network-former units Si or Al. Q^n_T is the central tetrahedron of a network former T with n bridging oxygens (BOs). m is the number of T′ tetrahedra connected to the central tetrahedron. To distinguish the structural units more clearly, the $Q^n_{Si}(m\text{Al})$ and $Q^n_{Al}(m\text{Si})$ units are separated into two groups: the first group consists of $Q^n_{Si}(m(=0)\text{Al})$ units, including $Q^4_{Si}(0\text{Al})$, $Q^3_{Si}(0\text{Al})$, $Q^2_{Si}(0\text{Al})$, $Q^1_{Si}(0\text{Al})$ and $Q^0_{Si}(0\text{Al})$; the second group consists of $Q^n_{Si}(m(\neq 0)\text{Al})$ units, including $Q^4_{Si}(4\text{Al})$, $Q^4_{Si}(3\text{Al})$, $Q^4_{Si}(2\text{Al})$, $Q^4_{Si}(1\text{Al})$, $Q^3_{Si}(3\text{Al})$, $Q^3_{Si}(2\text{Al})$, $Q^3_{Si}(1\text{Al})$, $Q^2_{Si}(2\text{Al})$, $Q^2_{Si}(1\text{Al})$ and $Q^1_{Si}(1\text{Al})$; the third group consists of $Q^n_{Al}(m(=0)\text{Si})$ units, including $Q^4_{Al}(0\text{Si})$, $Q^3_{Al}(0\text{Si})$, $Q^2_{Al}(0\text{Si})$, $Q^1_{Al}(0\text{Si})$ and $Q^0_{Al}(0\text{Si})$; and the fourth group consists of $Q^n_{Al}(m(\neq 0)\text{Si})$ units, including $Q^4_{Al}(4\text{Si})$, $Q^4_{Al}(3\text{Si})$, $Q^4_{Al}(2\text{Si})$, $Q^4_{Al}(1\text{Si})$, $Q^3_{Al}(3\text{Si})$, $Q^3_{Al}(2\text{Si})$, $Q^3_{Al}(1\text{Si})$, $Q^2_{Al}(2\text{Si})$, $Q^2_{Al}(1\text{Si})$, and $Q^1_{Al}(1\text{Si})$.

In the search for tetrahedral units, the wide distribution range of $Q^n_{Si}(m\text{Al})$ and $Q^n_{Al}(m\text{Si})$ units in the simulated glasses is calculated by using an Si–O and Al–O cut-off radii of 2.5 Å. The obtained distributions of Si and Al are presented in Table 2. The percentage of O present in the $Si^{[4]}$–O–$Si^{[4]}$, $Si^{[4]}$–O–$Al^{[4]}$ and $Al^{[4]}$–O–$Al^{[4]}$ bridges is calculated by the ratio of the number of O in the respective bondings over the total number of O, as shown in Table 3 along with the standard deviations calculated for the five samples. The majority of BOs reside in heteronuclear $Si^{[4]}$–O–$Al^{[4]}$ linkages, 30.5% in M-glass and 26.2% in P-glass, and a significant amount of homonuclear $Si^{[4]}$–O–$Si^{[4]}$ and $Al^{[4]}$–O–$Al^{[4]}$ bonds exist in both simulated glasses. It can be concluded, therefore, that irrespective of the force fields, the CMAS glass contains a non-negligible amount of $Al^{[4]}$–O–$Al^{[4]}$ bonds. To understand the distribution of other cations, we have further determined the presence of each cation type in the network on the basis of oxygen coordination. For example, the number of Si–O bonds present in the Si–O–Si bridges is calculated and its proportion among all Si–O bonds is considered as a percentage of Si in Si–O–Si. A similar procedure was followed for calculating the presence of other cations in different BO and non-bridging oxygen (NBO) environments. The results, summarised in Table 4 for P-glass, indicate that 30.6% of Si resides in Si–O–Si bonds, 32.9% in Si–O–Al bonds and 34.9% in Si–NBO bonds; 47.7% of Al resides in Si–O–Al bonds, 32.8% in Al–O–Al bonds and 12.6% Al–NBO bonds. This clearly indicates the presence of significant fractions of Al–O–Al and Al–NBO bonds in CMAS glass. It is worth mentioning here that the percentage of each cation is calculated based on its coordination rather than the charge contribution. For example, if an O atom in Si–O–Al is connected to Ca then, according to charge distribution, 50% of this O is considered to be connected to Si, 37.5% to Al and 12.5% to Ca. On the other hand, O is considered to be connected equally to all the three cations when calculated based on coordination. The latter method is considered in the present study. To visualise the distribution of Si–O–Al units, all possible tetrahedra with Si–O–Al bonds in a slice of 10 Å thickness are extracted from $Q^n_{Si}((m\neq 0)\text{Al})$ units and these are shown in Fig. 2a; a surface mesh is constructed around these atoms and shown in Fig. 2b to enhance the underlying regions. It is evident from the figures that the

Table 2 Distribution of Si and Al atoms (%) with respect to their neighbouring cations in the form of $Q^n(m\text{Al})$ units and $Q^n(m\text{Si})$ units

$Q^n_{Si}(m\text{Al})$ units' distribution			$Q^n_{Al}(m\text{Si})$ units' distribution		
	M-Glass	P-Glass		M-Glass	P-Glass
Q^0(0Al)	1.9 ± 0.7	2.8 ± 1.0	Q^0(0Si)	0.0	0.0
Q^1(0Al)	5.3 ± 0.5	8.0 ± 0.5	Q^1(0Si)	0.4 ± 0.4	0.5 ± 0.3
Q^1(1Al)	5.8 ± 1.2	6.6 ± 1.2	Q^1(1Si)	1.0 ± 0.9	0.7 ± 0.5
Q^2(0Al)	6.7 ± 2.0	8.6 ± 0.8	Q^2(0Si)	1.5 ± 0.5	0.8 ± 0.3
Q^2(1Al)	15.6 ± 1.4	16.3 ± 1.2	Q^2(1Si)	4.2 ± 1.3	3.3 ± 1.8
Q^2(2Al)	7.7 ± 1.3	6.9 ± 0.7	Q^2(2Si)	3.4 ± 0.9	4.2 ± 1.1
Q^3(0Al)	4.4 ± 1.1	4.6 ± 1.3	Q^3(0Si)	1.7 ± 0.8	1.2 ± 0.6
Q^3(1Al)	13.9 ± 3.1	12.4 ± 2.2	Q^3(1Si)	8.4 ± 2.6	5.6 ± 1.5
Q^3(2Al)	15.0 ± 1.5	11.3 ± 1.8	Q^3(2Si)	13.3 ± 0.8	10.2 ± 3.0
Q^3(3Al)	6.0 ± 1.1	2.9 ± 0.7	Q^3(3Si)	9.4 ± 0.8	7.1 ± 2.0
Q^4(0Al)	0.7 ± 0.3	0.7 ± 0.6	Q^4(0Si)	0.8 ± 0.4	0.2 ± 0.2
Q^4(1Al)	3.1 ± 0.8	2.8 ± 1.1	Q^4(1Si)	4.7 ± 1.7	3.2 ± 0.7
Q^4(2Al)	5.5 ± 0.8	4.6 ± 1.3	Q^4(2Si)	13.9 ± 1.8	7.8 ± 1.5
Q^4(3Al)	4.0 ± 1.4	3.3 ± 1.4	Q^4(3Si)	14.7 ± 2.0	11.2 ± 2.2
Q^4(4Al)	1.4 ± 0.9	0.5 ± 0.3	Q^4(4Si)	7.0 ± 1.7	4.5 ± 0.8

Table 3 Amount of O in Si–O–Si, Si–O–Al, Al–O–Al, Si–NBO and Al–NBO bonds in M-glass and P-glass.[a] Average coordination of non-framework cations based on the type of oxygen for P-glass. NBO stand for "non-bridging oxygen"

Sample name	$Si^{[4]}$–O–$Si^{[4]}$	$Si^{[4]}$–O–$Al^{[4]}$	$Al^{[4]}$–O–$Al^{[4]}$	Si–NBO	Al–NBO
M-Glass	14.1 (14.1)	30.5 (32.1)	8.5 (9.5)	33.1 ± 0.5	9.4 ± 0.4
P-Glass	14.2 (14.2)	26.2 (30.9)	7.0 (9.1)	32.9 ± 0.5	8.2 ± 0.4

	Average coordination of non-framework cations based on the type of O				
Cation	SiOSi/R	SiOAl/R	AlOAl/R	Si–NBO/R	Al–NBO/R
R = Ca	0.40 ± 0.02	1.25 ± 0.03	0.49 ± 0.03	3.01 ± 0.05	0.82 ± 0.06
R = Mg	0.14 ± 0.04	0.64 ± 0.07	0.39 ± 0.03	2.28 ± 0.10	0.87 ± 0.14

[a] The values inside the parentheses are the percentages of corresponding units irrespective of the coordination of the cations.

Table 4 Percentage of an atom type existing in different bonding states based on O and network-forming cations for P-glass

	Bridging oxygen			Non-bridging oxygen	
	56.0 ± 0.2			44.0 ± 0.2	
% of O	Si–O–Si	Si–O–Al	Al–O–Al	Si–O	Al–O
	14.4 ± 0.2	30.9 ± 0.3	10.6 ± 0.2	32.9 ± 0.2	8.2 ± 0.2
	Bridging oxygen			Non-bridging oxygen	
	63.5 ± 0.2			36.5 ± 0.2	
% of Si	Si–O–Si	Si–O–Al	Al–O–Al	Si–O	Al–O
	30.6 ± 0.3	32.9 ± 0.3	0	34.9 ± 0.2	0.0
	Bridging oxygen			Non-bridging oxygen	
	80.5 ± 0.3			19.5 ± 0.3	
% of Al	Si–O–Si	Si–O–Al	Al–O–Al	Si–O	Al–O
	0.0	47.7 ± 0.4	32.8 ± 0.6	0.0	12.6 ± 0.3
	Bridging oxygen			Non-bridging oxygen	
	34.5 ± 0.3			65.5 ± 0.3	
% of Ca	Si–O–Si	Si–O–Al	Al–O–Al	Si–O	Al–O
	6.5 ± 0.1	20.0 ± 0.2	8.0 ± 0.2	48.2 ± 0.4	13.2 ± 0.4
	Bridging oxygen			Non-bridging oxygen	
	25.4 ± 1.0			74.6 ± 1.0	
% of Mg	Si–O–Si	Si–O–Al	Al–O–Al	Si–O	Al–O
	3.0 ± 0.3	13.7 ± 0.5	8.6 ± 0.5	49.6 ± 0.3	18.9 ± 0.9

distribution of Si–O–Al is not uniform and that such linkages form as cluster regions in the CMAS glass of the present composition.

3.3 Distribution of SiO_2 units

The distribution of $Q^n_{Si}((m < n)Al)$ units indicates that a significant amount of Si is present as Si–O–Si bonds (Table 2). The $Q^3_{Si}(0Al)$ and $Q^4_{Si}(0Al)$ units should be surrounded by a larger number of neighbouring Si tetrahedra, indicating the possible formation of a silica-rich cluster region. Table 2 shows that more than 5% of Si exists in such $Q^3_{Si}(0Al)$ and $Q^4_{Si}(0Al)$ cluster regions. From Table 4, it is revealed that, overall, 30.6% of Si resides in Si–O–Si bonds. All the Si tetrahedra in the Si–O–Si bonds in a 10 Å thick slice are extracted and their atomistic distribution is presented in Fig. 2c; a surface mesh is created around these atoms in order to highlight the cluster regions as presented in Fig. 2d.

3.4 Distribution of Ca, Mg and NBO

The $Q^n_{Si}(m\text{Al})$ and $Q^n_{Al}(m\text{Si})$ units, except n = 4, are associated with NBOs, since CMAS does not have any dangling bonds. Overall, the fractions of BOs and NBOs in P-glass are calculated to be 56% and 41% of the total oxygen content, respectively (Table 4). Interestingly, we observe that 19.5% of NBOs are associated with Al in Al–NBO bonds. A major portion of NBOs is, however, still associated with Si atoms in Si–NBO bonds, *i.e.* 80.5% of the total NBOs, which is in agreement with the experimental results of Allwardt *et al.*[48] and Lee *et al.*[24] and MD simulations by Pedone *et al.*[49] It is known that the addition of network-modifying cations selectively depolymerizes the silicate network, leading to the formation of Si–NBO bonds.[50] When intermediate cations (conditional network formers) are present in silicate glasses, a portion of the non-framework cations depolymerizes the structure while the remaining portion participates in charge compensation.

Table 2 reveals that a large portion of NBOs, in principle connected to R (R ∈ {Ca,Mg}) atoms, exists in CMAS glass. Among various possible structural motifs, $Q^{n<2}_{Si}(m\text{Al})$ and $Q^{n<2}_{Al}(m\text{Si})$ units have the highest density of NBOs and their analysis could reveal the distribution of R atoms in the CMAS glass. These motifs sum to around 18% of Si units that are involved in higher density regions of NBOs, whereas less than 1% of Al is found in a higher density region of NBOs. In addition, Table 4 reveals that approximately 48.2% and 13.2% of Ca is connected to Si and Al, respectively, through NBOs. This indicates that up to 65.5% of Ca is acting as a network modifier and 35% of Ca as a charge compensator. On the other hand, 74.6% of Mg (Si–NBO: 49.6%; and Al–NBO: 18.9%) behaves as a network modifier and 25.4% of Mg as a charge compensator. Quantum-chemical calculations revealed that the energy penalty for the formation of Ca–O–Al is much smaller than that of Na–O–Al formation, and the energy penalty for the formation of Mg–O–Al is much smaller than that for Ca–O–Al.[24,51] This indicates that the presence of high-field-strength modifier cations that prefer to have lower coordination increases the probability of coordinating with available sites of high negative charge. Since Al–NBO has a higher accumulated negative charge of −1.25 valence units (VU) compared to Si–NBO (−1.0 VU), the high field strength Mg cation has a greater preference to coordinate with Al–NBO than a comparatively lower field strength Ca cation.[24] This suggests that, between the two available non-framework cations, Ca prefers to be the charge compensator for Si–O–Al bonds, while Mg prefers to be the network modifier. Initially, the distribution of R atoms is analysed with respect to the bonds formed with BO and NBO atoms, presented in Table 3. However, such an analysis does not provide a complete environment of R, so the distribution of R atoms is further analysed by categorising the O atoms based on both the coordination and their surrounding environment with respect to all other cation types. The most frequently occurring environments of O based on the number and type of neighbouring cations are computed and the values are presented in Table 5. The schematic representation of each type of O is shown in Fig. 5b. In order to distinguish the role of Ca and Mg in the CMAS glass, the Ca and Mg atoms are further separated based on their neighbouring atoms, in a similar manner to the analysis performed for O. The percentage of non-framework cations is computed based on the number and type of BOs and NBOs with which they are connected, see Table 6. From these analyses, it can be deduced that on average each Ca or Mg is connected to ∼3 Si–NBO. However, Ca shows a slightly greater preference than Mg to bond with Si–NBO, whereas Mg prefers to bond with Al-NBO (Table 4). Fig. 2e shows the atomistic distribution of R atoms along with their neighbours in a slice with a thickness of 10 Å. A surface mesh is created to enhance the visibility of the R-rich channel regions and is presented in Fig. 2f.

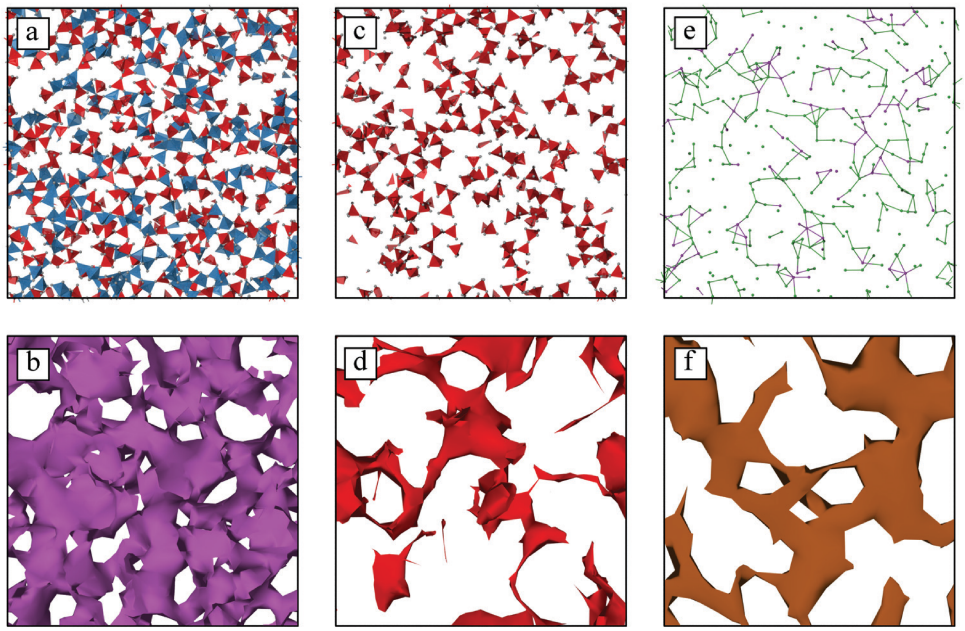

Fig. 2 Identification of different cluster regions in a slice of width 10 Å in CMAS glass. (a) All Si (red) and Al (blue) tetrahedra involved in Si–O–Al bonds from $Q^n_{Si}(m(\neq 0)Al)$ units are separated. (b) A surface mesh is created out of all the atoms in (a) and is shown in purple. (c) All Si (red) tetrahedra involved in Si–O–Si bonds from $Q^n_{Si}(m(\neq n)Al)$ units are separated. (d) A surface mesh is created out of all the atoms in (c) and is shown in red. (e) All Ca (apple green) and Mg (violet) atoms are separated and artificial bonds are created between them with a bond length of 4.5 Å. (f) A surface mesh is created out of all the atoms in (e) and is shown in brown.

Table 5 Amount of different types of oxygen in CMAS glass. The schematic representation of these oxygen types is shown in Fig. 5b

Sample	Type 1	Type 2	Type 3	Type 4	Type 5	Type 6	Type 7	Type 8	Type 9
P-Glass	18.34 ± 0.34	7.65 ± 0.01	4.14 ± 0.19	6.80 ± 0.10	4.44 ± 0.03	14.21 ± 0.28	16.28 ± 0.08	5.22 ± 0.19	1.5 ± 0.17
M-Glass	18.98 ± 0.24	7.73 ± 0.06	4.44 ± 0.14	7.78 ± 0.0	4.19 ± 0.22	15.25 ± 0.11	15.24 ± 0.24	6.08 ± 0.11	1.8 ± 0.07

Table 6 Percentage of non-framework cations (R) bonded to oxygen based on its environment in P-glass (only the most frequently occurring oxygen environments are presented)

0SiO	1SiO	2SiO	3SiO	4SiO	5SiO
3.02 ± 0.22	13.55 ± 0.42	25.95 ± 1.14	25.54 ± 0.8	19.09 ± 0.59	9.71 ± 0.78
0AlO	1AlO	2AlO	3AlO	0SiOSi	1SiOSi
40.70 ± 1.09	39.01 ± 0.89	17.32 ± 0.96	2.6 ± 0.16	71.07 ± 0.45	23.76 ± 0.59
0SiOAl	1SiOAl	2SiOAl	0AlOAl	1AlOAl	2AlOAl
35.04 ± 0.83	32.97 ± 0.81	20.08 ± 0.62	66.45 ± 0.7	23.39 ± 0.75	7.64 ± 0.18

3.5 Triclusters

According to Zachariasen,[9] oxygen is connected to a maximum of two network-forming cations at the corner of a tetrahedron. Despite this, oxygen can also connect with three network-forming cations and such oxygen sites are called triclusters.[6,9,52] The formation of triclusters (OT_3, T ∈ {Si,Al}) has already been documented for alkali/alkaline-earth aluminosilicate glass systems.[6,53–56] Triclusters are supposed to have a crucial role in crystallization and to have a significant influence on transport properties in several aluminosilicate glasses.[54] It has been pointed out that thermal fluctuations may possibly lead to the formation of triclusters.[6,54] However, the favourable conditions for their formation are not yet fully understood. In the present study, a significant number of oxygen atoms (~2%) is found to bond with three network-forming cations at a given time. The proportions of different possible triclusters of the CMAS glass predicted by the random network model[54] and computed by MD simulations are presented in Table 7. According to the random network model, 8% of OAl_3 and 29.4% of OAl_2Si triclusters are predicted; however, higher values of 60.7% and 37.5%, respectively, are obtained by MD simulations. It is also observed in the present study that more OAl_3 and OAl_2Si triclusters are formed at the expense of $OAlSi_2$ and OSi_3

Table 7 Percentage of various triclusters in CMAS glass

Tricluster	OAl_3	OAl_2Si	$OAlSi_2$	OSi_3
Random network model (%)	8.0	29.4	40.8	21.8
MD simulation (%)	46.9 ± 4.5	48.5 ± 1.7	4.5 ± 3.0	0

triclusters. This signifies that the formation of triclusters is not random but could be favoured by some particular environments. A schematic representation of OAl_3 and OAl_2Si triclusters is presented in Fig. S5, ESI.†

4. Discussion

As described by Stebbins *et al.*,[25] alkali or alkaline-earth aluminosilicate glasses with a Si/Al ratio < 1 favour the development of Al–O–Al bonds even in the presence of Si. On the other hand, complete avoidance of Al–O–Al bonds has been assumed in some models of aluminosilicate glass structures for Si/Al ≥ 1.[57] The MD simulation results of the CMAS glass (Si/Al = 1.5) in the present study clearly reveal that a notable amount, 32.8%, of Al exists in Al–O–Al bonds (see Table 4). Deconvolution analysis of the ^{29}Si MAS-NMR spectra for CMAS glass[33] from an earlier experimental study revealed that 60% of Al exists in Al–O–Al bonds. This value is twice that of the simulated glass. Despite this difference in the amount, both methods show that a significant amount of Al is present in Al–O–Al bonds. The discrepancy in the calculated amount of Al between the simulation and NMR results is attributed to the assumptions made for the spectral decomposition. The existence of Al–NBO bonds is not considered during the deconvolution of NMR results whereas the simulation results show that around 13% of Al is present in Al–NBO bonds. Nevertheless, identifying the reasons behind the formation of Al–O–Al and Al–NBO bonds in alkaline-earth aluminosilicate glasses remains challenging. A preliminary attempt has been made, therefore, to understand the formation of Al–O–Al and Al–NBO bonds in CMAS glass based on general theories of the formation of Si–O–Si, Si–O–Al and Si–NBO bonds, taking into account the preferred coordination numbers of Si, Al and R (R $\in$ {Ca,Mg}) atoms. In addition, a support for the recently proposed EMRN model[33] has been provided considering the formation of cluster regions in alkaline-earth aluminosilicate glass.

4.1 Formation of Si–O–Al and SiO_2-rich regions

It is known that Si is a strong network former and that Al also acts as a network former in the presence of other network formers along with charge compensators.[58] In the CMAS glass system, a majority of Si and Al exhibit perfect tetrahedral coordination, and constitute the primary framework units. According to Lowenstein, when Al is introduced into the Si–O–Si network, each Al prefers to share its O with Si rather than another Al, and thus Si–O–Al bonds are preferred in aluminosilicate glasses.[11] *Ab initio* studies[59,60] and energy calculations of quadrupolar interactions[61] confirm that Si–O–Al bonds are energetically more favourable than both Si–O–Si and Al–O–Al bonds. Experimental studies have also shown that ^{IV}Al prefers to occupy regions with the most polymerized structural units.[58] Nevertheless, the preference of Al for Q^4 sites also depends on several factors, as explained by Merzbacher *et al.*[30] The tendency for Al to reside in $Q^4_{Si}(m\text{Al})$ sites decreases if Ca and Mg are present instead of alkali metals as modifiers and charge compensators. The $Q^n_{Si}(m \neq 0\text{Al})$ unit distribution for CMAS glass (Table 2) confirms the formation of a large number of Si–O–Al bonds. The following discussion proposes a description of the formation of Si–O–Al and Si–O–Si regions in the present CMAS glass.

In general, Si with +4 valence units (VUs) is charge balanced by 4 O atoms: each O contributes −1 VU to the Si, such that the charge neutrality requirement of O is fulfilled in Si–O–Si bonds. However, if Al (+3 VU) is in tetrahedral coordination then it can contribute only +0.75 VU to each neighbouring O. In such a case, O is lacking the +0.25 VU required to achieve charge neutralisation in Si–O-Al bonds. If an R atom with +2 VU is going to fulfil this imbalanced charge in the Si–O–Al bonds, then each R atom should connect to eight of such Si–O–Al BOs. In that case, the R^{2+} cations will have 8 first neighbouring BOs and 16 first neighbour network-forming cations (Si or Al). However, Ca ions with an ionic radius of 0.99 Å prefer to adopt a coordination number lower than eight, whereas Mg ions with an ionic radius of 0.65 Å prefer a coordination number between four and six.[62,63] In order to maintain the number of O neighbours lower than eight, the modifier cation should contribute more than +0.25 VU with some of its neighbours. In aluminosilicate glasses, there are only three possibilities available for having more than −0.25 VU at the O sites, these are Si–NBO (−1 VU), Al–O–Al (−0.5 VU) and Al–NBO (−1.25 VU). Of these three choices, Si–NBO is energetically more favourable.[23] We assumed that all Al are in Si–O–Al linkages, therefore, the former possibility (Si–NBO) is the only option to maintain the R atom coordination <8. Ultimately, Si–O–Al formation requires additional Si and R cations. In the present CMAS glass composition, there are fewer Al atoms than Si and R atoms (Al/Si < 1 and R/Al < 1), which should be enough to satisfy Lowenstein's rule by having 100% of Al in Si–O–Al bonds if considering only charge-balance requirements. However, as discussed earlier, some portion of Si is additionally required to form Si–O–Ca in order to form Si–O–Al. The 12.9% (mol) of Al_2O_3 requires 12.9% of RO and 25.8% SiO_2 to have a completely polymerized structure and maintain Lowenstein's rule. In this case, the remaining 12.9% of SiO_2 is not enough for the left over 35.5% RO to adopt a stabilized structure. In this situation, the Si–O–Al linkages are broken and Al–O–Al linkages and R-channel regions are formed instead; the necessary conditions for the formation of both Al–O–Al and R-channel regions are discussed in the following sections. The R atoms are required for Al–O–Al and R-channel regions but not for Si–O–Si linkages. Hence, Si–O–Si bonds are preferred where the R atoms are not available, as the R atoms are locked in the above two sites. Fig. 2b and e support the formation of SiO_2-rich regions in the CMAS glass. It is clear that charge compensators are needed to promote the formation of Si–O–Al bonds, which are then surrounded by a majority of R-rich channel regions together with NBOs. The excess Si prefers, therefore, to form Si–O–Si

bonds instead of Si–O–Al. Since Si–O–Si linkages do not require any charge compensator, they can potentially form homonuclear clusters anywhere in the structure.

4.2 Formation of Ca/Mg-rich channels

As we discussed above, the R atoms prefer to maintain a coordination number lower than eight and favour less dense, first-neighbour, network-forming cations. To attain this, each R atom attempts to connect with more than one Si–NBO. At the same time, each Si–NBO prefers to be shared by more than one R atom. In the present CMAS glass, it is also calculated that $26.0 \pm 1.0\%$ of R atoms are connected to 2 Si–NBO, $25.5 \pm 0.8\%$ to 3 Si–NBO and $19.1 \pm 0.6\%$ to 4 Si–NBO (Table 6). On average, each Ca and Mg atom are connected to 3 and 2.3 Si-NBOs, respectively (Table 3), which is, qualitatively, in agreement with Greaves.[11] Each Si–NBO has -1 VU of charge but each R atom can only share < -1 VU to maintain its preferential coordination. A majority of R atoms prefer, therefore, to bond with more than one Si–NBO. Consistently, in the present CMAS glass, we observe around $30.5 \pm 0.3\%$ of O atoms with an environment of either Si–NBO–2R or Si–NBO–3R (see Table 4). To sum up, each R atom compensating the imbalanced charge at the O site in Si–O–Al linkages is also connected to more than one Si–NBO, and each of these Si–NBO atoms attracts more than one R atom. The interdependent bonding requirements of R and Si–NBO combine, therefore, to form R-rich channels in accordance with the present results.

4.3 Formation of Al–O–Al bonds

A simulation snapshot of P-glass, Fig. 4, clearly shows the existence of Al–O–Al bonds in the CMAS glass. Based on the presented results, 32.8% of Al and 10.6% of O exist in Al–O–Al bonds, such that the Lowenstein's Al-avoidance rule is breached in the present CMAS glass composition. It has been reported that increasing the Si/Al ratio increases the quantity of $Q^4_{Al}(4Si)$ or $Q^4_{Al}(3Si)$ units and decreases Al–O–Al bond formation.[26] In addition, Oestrik *et al.*[64] have mentioned that a framework structure with Si/(Si + Al) less than 0.5 must violate the alumina avoidance rule and contain some Al–O–Al bonds. The possibility of the formation of Al–O–Al bonds in CMAS glass with a lower Al content of Si/Al = 1.7 and Si/(Si + Al) = 0.6 is described as follows.

The CMAS glass structure consists primarily of three regions: (i) a region enriched in Si–O–Al bonds; (ii) a region enriched in Si–O–Si bonds and (iii) an NBO-enriched region with non-network-forming cations. Identifying the distribution of $Q^n_{Al}(m\mathrm{Si})$ units in the possible three regions can help to explore the reasons behind the formation of Al–O–Al bonds in aluminosilicate glasses. The following assumptions are, therefore, made based on the distribution of $Q^n_{Al}(m\mathrm{Si})$ units: (i) $Q^0_{Al}(0\mathrm{Si})$ units are confined to the R-rich non-network region since these units do not have any BOs; (ii) a majority of Q^1_{Al} and Q^2_{Al} units are present at the border of the R-rich non-network region; (iii) Q^3_{Al} units are either located in the Si–O–Al enriched region or at the interface of Si–O–Al and R-rich channel regions; (iv) Q^4_{Al} units reside in the Si–O–Al enriched region since these units contain only BOs. Table 2 shows that a majority of Al atoms are in $Q^4_{Al}(m\mathrm{Si})$ and $Q^3_{Al}(m\mathrm{Si})$ distributions, which indicates that Al prefers to be surrounded by either three or four BOs, with the effect that most Al–O–Al bonds are located in the Si–O–Al region. In addition, a small value obtained on summing the $Q^1_{Al}(0\mathrm{Si})$, $Q^2_{Al}(0\mathrm{Si})$ and $Q^2_{Al}(1\mathrm{Si})$ units indicates that fewer Al–O–Al bonds are located near to the R-rich, non-network region.

According to Lowenstein, if all the Al in the CMAS glass are connected to Si through a BO such as Si–O–Al and the required charge for neutralization is provided by R atoms, then there will be an excess of Si and R atoms left in the system, because $\mathrm{Si/Al} > 1$ and $\mathrm{R/Al} > 0.5$. Since R atoms prefer Si–NBO, all the remaining Si atoms after the formation of Si–O–Al bonds can readily connect to R through NBOs. Nevertheless, there should still be additional R atoms remaining in the system because the ratio of leftover R to leftover Si cations after the formation of Si–O–Al is still greater than 1. There will be no option left other than breaking some of the Si–O–Al bonds in order for R atoms to achieve their preferred coordination. The broken Si–O–Al bonds can become either Si–NBO and Al–NBO or Si–O–Si and Al–O–Al. In the former reaction, Si–NBO is more stable and in the latter reaction Si–O–Si is more stable. Whether or not the former or latter reaction occurs is largely dependent on the R atoms available near to them. The former reaction takes place if the broken Si–O–Al bond is near to an R-rich region because R atoms prefer to be formed as R-rich channels. The latter reaction takes place if the available R atoms are not located in clusters. To this end, we can say that even though there are sufficient Si atoms for Al atoms to form Si–O–Al bonds, the presence of excess R atoms in the network prevents the formation of Si–O–Al bonds and creates more non-bridging bonds. Since R atoms prefer to bond with Si–NBO rather than Al–NBO,[54] the excess R atoms connect to Si through NBOs. Therefore, the left over Al has no choice other than to form Al–O–Al bonds. Moreover, each O atom in an Al–O–Al linkage, with a charge imbalance of -0.5 VU (more than the -0.25 VU charge required by an R atom to keep its coordination lower), promotes the formation of Al–O–Al bonds even though it is energetically not favourable.[12,56] Hence, the Lowenstein Al-avoidance rule is flouted for a high concentration of R atoms. As it has been reported for CMAS-type glass systems,17 the strong affinity between Mg^{2+} and Al–O–Al plays a major role in stabilizing the Al–O–Al bonds.[26] In fact, for the present CMAS glass, both Ca^{2+} and Mg^{2+} cations are important in stabilizing the Al–O–Al bonds (Table 4).

4.4 Formation of Al–NBO bonds

The reported results, that both 8.2% of O and 13% of Al exist in Al–NBO bonds, show that a significant number of Al–NBO bonds occurs in the present CMAS glass. It is clear from the earlier discussion that the accumulation of a negative charge at O sites is higher in Al–O–Al and Al–NBO bonds than in Si–O–Al bonds. It was also argued that Al–O–Al bonds prefer to be formed when the R-channel region is not in the vicinity. After the decomposition of the Si–O–Al linkage, the O prefers to stay as Al–NBO rather than Al–O–Al in the R-rich channel in order to

fulfill the requirement of lower neighbouring cation density around R. In addition, since Al–NBO can share a charge of −1.25 VU to 2 or 3 R atoms, the R-rich channel promotes the formation of Al–NBO rather than Al–O–Al.

Experimental evidence for the presence of a significant fraction of Al–NBO bonds (∼10%) in SiO_2-rich (> 40 mol%) RE_2O_3–Al_2O_3–SiO_2 glasses (RE = Y, Lu, Sc) was provided very recently for the first time by employing ^{17}O MAS-NMR and MD simulations.[23,65] It was further reported that Al–O–Ca bonds in Ca-aluminosilicate glasses can only be seen for very high Al concentrations (*e.g.*, Al/Si ≥ 3).[48] Moreover, the work of Jaworski *et al.*[23] provides evidence for the existence of Al–NBO bonds. It was reported that, in the presence of high-field-strength modifier cations, the formation of highly coordinated Al and/or Al–NBO is dominant.[16] A significant fraction of Al–O–R bonds is observed in the present study even though the concentration of Al is lower than Si (Al/Si = 0.66). Calculation of the fraction of modifier cations (Tables 3 and 4) linked to the NBOs further illustrates that most of the Al–NBO bonds are connected with three modifier cations. The required charge compensation of 1.25 VU for Al–NBO is possibly provided by either two Mg and one Ca, or one Mg and two Ca modifier atoms. Fig. 3 shows the simulation snapshot of P-glass (some of the atoms are removed for clarity), in which it can be seen that an R atom is connected to both BOs and NBOs, especially Al–NBOs.

4.5 Formation of triclusters

We discussed that after the Si–O–Al linkages are broken, the Al prefers to form Al-NBO linkages near the R-rich channel, whereas it prefers to form Al–O–Al if it is located away from the R-rich channel. In the places where the Al–O–Al bond is formed and R atoms are not available for balancing the negative charge, then the O atom of Al–O–Al is potentially ready to form a tricluster by bonding either with another Al or nearby Si. From the previous discussion, as the R atoms are locked in a channel region, other regions must have a shortfall of R atoms. The extra Al atoms in such regions form Al–O–Al, with a charge deficiency of 0.5 VU, which can be compensated by neighbouring Si or Al, by forming a tri-cluster with either 1 Si and 2 Al or 3 Al. In the present CMAS glass, it was shown that around 3% of the O is in triclusters, 50% of which is in 3 Al triclusters while the other 50% is in 2 Al and one Si triclusters. Although an exact relationship is not established between the formation of triclusters and fivefold-coordinated Al, some interesting observations may be made from the present study. A total of 11.7 ± 1.8% of Al atoms is found in five-fold coordination and 72.4 ± 3.1% of these Al are associated with the tricluster oxygen. This shows a strong affinity towards the formation of tricluster and fivefold coordinated Al. Such a behaviour has already been observed in several previous studies.[66,67] This can possibly be explained by the stoichiometry, since the O atoms at the tricluster sites attain a minimum of +0.25 VU charge imbalance; therefore, one of these Al can adopt 5-fold coordination such that the charge can be balanced at the tricluster sites. However, the presence of the fivefold coordinated Al was not experimentally observed in the investigated compositions (Fig. S6, ESI†).[33] This is possibly due to the different thermal histories used in the experiment and simulation.

4.6 Extended modified random network model

The distribution of $Q^4_{Si}(3Al)$, $Q^4_{Si}(4Al)$, $Q^4_{Al}(3Si)$ and $Q^4_{Al}(4Si)$ units validates the formation of a heteronuclear cluster region, as shown in Fig. 2a and b. The distribution of $Q^4_{Si}(3Si)$ and $Q^4_{Si}(4Si)$ units suggests the formation of SiO_2-rich homonuclear regions, as shown in Fig. 2c and d. Furthermore, the distribution of $Q^0_{Si}(0Al)$, $Q^1_{Si}(0Al)$, $Q^2_{Si}(0Al)$, $Q^0_{Al}(0Si)$, $Q^1_{Al}(0Si)$ and $Q^2_{Al}(0Si)$ units validates the formation of an R-rich channel region with a higher density of NBOs (see Fig. 2e and 2f). Fig. 4 shows that the total structure is a composition of three separate regions. This suggests that the glass structure regions consisting of framework and non-framework units are mutually distinguishable which supports the basic concept of the MRN model. According to the MRN model, the glass network structure consists of a network structure region with network-forming units and BOs and a channel region consisting of modifier cations and NBOs. Nevertheless, the distribution of framework units in CMAS glass suggests that the network-structure region of the MRN model is separated into heteronuclear and homonuclear regions, which generally

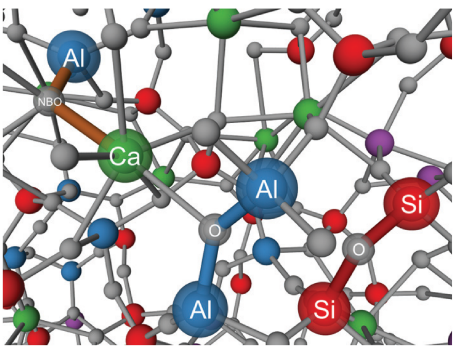

Fig. 3 Atomic structure of the CMAS glass showing the presence of Al–O–Al, Si–O–Si, and Al–NBO bonds.

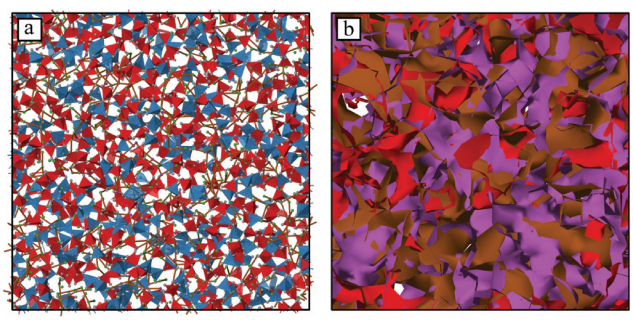

Fig. 4 Distribution of modifier cations and the identification of channel regions (a): all atoms within a slice 10 Å thick. Si and Al tetrahedron are represented in red and blue, respectively. (b) Surface meshes created separately for all the atoms in the Si–O–Si (red), Si–O–Al (violet) and R–O (brown) bonds.

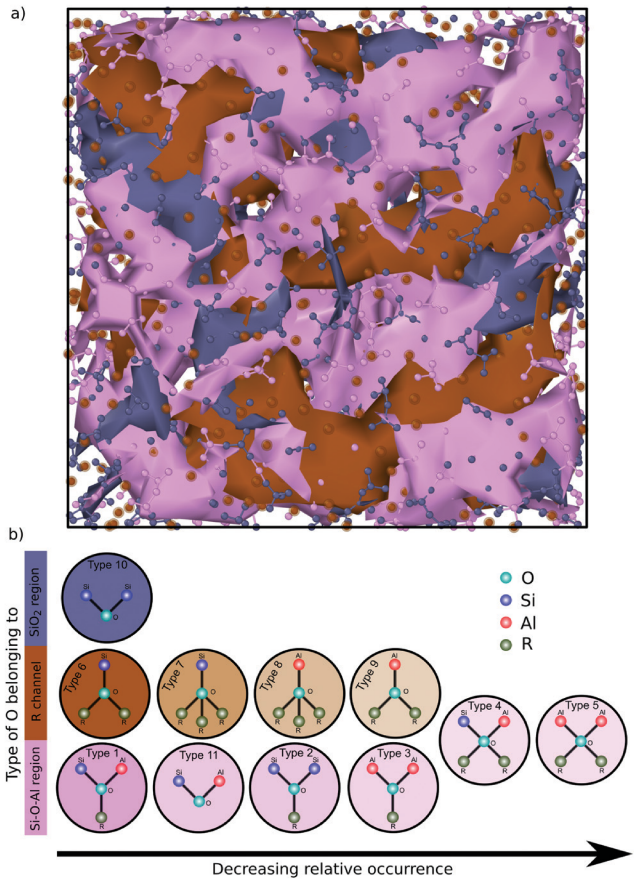

Fig. 5 (a) CMAS-M0 glass with the Si–O–Al (pink), Si–O–Si (silver) and R-rich channel (brown) regions represented. (b) Schematic diagrams of types of possible oxygen atoms and their relative occurrence in the region. The background colour of each oxygen type indicates the r region where a majority of these types of atoms can be found. The intensity of background colour represents the relative occurrence of the specified oxygen type.

contain $Q^n_{Si}(m(\neq 0)Al)$ and $Q^n_{Si}(m(=0)Al)$ units, respectively. Therefore, the MRN model, which was originally proposed by Greaves[5,11] for alkaline-earth aluminosilicate glasses, may be extended in order to better explain the distribution of structural units in glasses. In this regard, the EMRN (Extended Modified Random Network) model is proposed. The presence of the three cluster regions, heteronuclear, homonuclear and channel regions, is evidenced in Fig. 5a after separating the atoms into three groups containing Si–O–Al, Si–O–Si and R–O bonds. Furthermore, the atom types based on the environment are schematically shown in Fig. 5b and categorised based on their preference to reside in one of the three regions. The greater the intensity of the background colour of an atom type, the higher the probability of its occurrence in that region. Such classification of oxygen based on its environment complements the EMRN model. This model supports the formation of Al–O–Al bonds in clusters of hetero-nuclear units when Si–NBO bonds are present in sufficiently high concentrations. However, the distribution of framework and non-framework cations is highly dependent on the Si/Al and R/Al ratios; the validity, limits and conditions of the EMRN model therefore warrant further investigation.

5. Conclusions

A careful study has been performed to investigate the distribution of framework and non-framework structural units in alkaline-earth aluminosilicate (CMAS) glass using MD simulations. The influence of various parameters (interatomic potential, sample size, sample preparation method and cooling rate) on the distribution of structural units is studied and the results obtained are found to be consistent. Classification of oxygen based on its environment for CMAS glass indicates that the glass structure consists of clusters of SiO_4/AlO_4 units, SiO_4 units and R-atoms (Mg and Ca) along with NBOs. Owing to the preferred sharing of R^{2+} cations with Si–O–Al and Si–NBO bonds, these cations control the continuous cross-linking of SiO_4 and AlO_4 units and promote the formation of Si–O–Al enriched heteronuclear regions. The R-rich regions are formed because of the interdependent bonding requirement between charge compensating R (each R atom requires more than one Si–NBO) and Si–NBO atoms (each Si–NBO atom requires more than two R atoms). After forming Si–O–Al and Si–NBO bonds, the excess silicon atoms prefer to form silica-enriched regions which do not require any stabilizer, providing support for our proposed EMRN model. According to this model, in the absence of Si–NBO bonds in the heteronuclear SiO_4/AlO_4 cluster region, the presence of R atoms increases the formation of Al–O–Al bonds over continuous Si–O–Al bonds in order to lower the coordination number of the R atoms and to ensure charge neutrality. On the other hand, O prefers to form Al–NBO bonds rather than Al–O–Al in the R-rich channel to fulfil the requirement of a lower neighbouring-cation density around the R atoms.

Conflicts of interest

There are no conflicts to declare.

Acknowledgements

A. R. A. and S. B. would like to thank Dr Muraleedharan K., Director, CSIR-CGCRI for his strong support and encouragement. A. R. A. gratefully acknowledges the financial support of the Budapest Neutron Centre, Hungary, for allotting beam time and financial support (BRR_407) under the NMI3-II program. Part of this work was developed in the scope of the CICECO-Aveiro Institute of Materials (UID/CTM/50011/2013) project, and funded by FEDER funds through the Operational Programme Competitiveness Factors (COMPETE 2020) and the Portuguese Foundation for Science and Technology (FCT). S. G. would like to thank the German Research Foundation (DFG) for financial support through the priority program SPP 1594 "Topological Engineering of Ultra-Strong Glasses" (project BI1453/1-2). Simulations were performed with computing resources granted by RWTH Aachen University under project rwth0297.

References

1 M. Tiegel, A. Herrmann, C. Russel, J. Korner, D. Klopfel, J. Hein and M. C. Kaluza, *J. Mater. Chem. C*, 2013, **1**, 5031–5039.

2 A. R. Allu, S. Balaji, D. U. Tulyaganov, G. C. Mather, F. Margit, M. J. Pascual, R. Siegel, W. Milius, J. Senker, D. A. Agarkov, V. V. Kharton and J. M. F. Ferreira, *ACS Omega*, 2017, **2**, 6233–6243.

3 A. Brehault, D. Patil, H. Kamat, R. E. Youngman, L. M. Thirion, J. C. Mauro, C. L. Corkhill, J. S. McCloy and A. Goel, *J. Phys. Chem. B*, 2018, **122**, 1714–1729.

4 K. Januchta, R. E. Youngman, A. Goel, M. Bauchy, S. L. Logunov, S. J. Rzoska, M. Bockowski, L. R. Jensen and M. M. Smedskjaer, *Chem. Mater.*, 2017, **29**, 5865–5876.

5 S. Sukenaga, P. Florian, K. Kanehashi, H. Shibata, N. Saito, K. Nakashima and D. Massiot, *J. Phys. Chem. Lett.*, 2017, **8**, 2274–2279.

6 S. K. Lee and S. Ryu, *J. Phys. Chem. Lett.*, 2018, **9**, 150–156.

7 M. M. Smedskjaer, J. C. Mauro, J. Kjeldsen and Y. Yue, *J. Am. Ceram. Soc.*, 2013, **96**, 1436–1443.

8 A. A. Reddy, D. U. Tulyaganov, G. C. Mather, S. Rodr, S. Das, M. J. Pascual, F. Mun, J. Senker and J. M. F. Ferreira, *J. Phys. Chem. C*, 2015, **119**, 11482–11492.

9 W. H. Zachariasen, *J. Am. Chem. Soc.*, 1932, **54**, 3841–3851.

10 G. N. Greaves and K. L. Ngai, *Phys. Rev. B: Condens. Matter Mater. Phys.*, 1995, **52**, 6358–6380.

11 G. N. Greaves, *J. Non-Cryst. Solids*, 1985, **71**, 203–217.

12 W. Loewenstein, *Am. Mineral.*, 1954, **39**, 92–96.

13 M. F. Ando, O. Benzine, Z. Pan, J.-L. Garden, K. Wondraczek, S. Grimm, K. Schuster and L. Wondraczek, *Sci. Rep.*, 2018, **8**, 5394.

14 A. Gaddam, H. R. Fernandes, B. Doumert, L. Montagne and J. M. F. Ferreira, *Phys. Chem. Chem. Phys.*, 2017, **19**, 26034–26046.

15 A. Gaddam, H. R. Fernandes and J. M. F. Ferreira, *RSC Adv.*, 2015, **5**, 41066–41078.

16 S. K. Lee, H.-I. Kim, E. J. Kim, K. Y. Mun and S. Ryu, *J. Phys. Chem. C*, 2016, **120**, 737–749.

17 K. E. Kelsey, J. R. Allwardt and J. F. Stebbins, *J. Non-Cryst. Solids*, 2008, **354**, 4644–4653.

18 D. R. Neuville, L. Cormier and D. Massiot, *Chem. Geol.*, 2006, **229**, 173–185.

19 J. F. Stebbins, S. K. Lee and J. V. Oglesby, *Am. Mineral.*, 1999, **84**, 983–986.

20 E. Yildirim and R. Dupree, *Bull. Mater. Sci.*, 2004, **27**, 269–272.

21 S. Lee and J. Stebbins, *Am. Mineral.*, 1999, **84**, 937–945.

22 M. Moesgaard, R. Keding, J. Skibsted and Y. Yue, *Chem. Mater.*, 2010, **22**, 4471–4483.

23 A. Jaworski, B. Stevensson and M. Eden, *Phys. Chem. Chem. Phys.*, 2015, **17**, 18269–18272.

24 S. K. Lee and J. F. Stebbins, *Geochim. Cosmochim. Acta*, 2006, **70**, 4275–4286.

25 J. Stebbins, P. Zhao and X. Cheng, *Am. Mineral.*, 1999, **84**, 1680–1684.

26 S. Y. Park and S. K. Lee, *Geochim. Cosmochim. Acta*, 2012, **80**, 125–142.

27 W. Lothar, P. Zhiwen, P. Theresia, E. Andreas, M. T. Scott, S. Marek, M. Matthieu, H. Uwe, D. Joachim and G. G. Neville, *Adv. Sci.*, 2018, **5**, 1700850.

28 S. Keun and J. F. Stebbins, *Geochim. Cosmochim. Acta*, 2009, **73**, 1109–1119.

29 S. K. Lee and J. F. Stebbins, *J. Phys. Chem. B*, 2000, **104**, 4091–4100.

30 C. I. Merzbacher, B. L. Sherriff, J. S. Hartman and W. B. White, *J. Non-Cryst. Solids*, 1990, **124**, 194–206.

31 A. Jaworski, B. Stevensson, B. Pahari, K. Okhotnikov and M. Eden, *Phys. Chem. Chem. Phys.*, 2012, **14**, 15866–15878.

32 K. Okhotnikov, B. Stevensson and M. Eden, *Phys. Chem. Chem. Phys.*, 2013, **15**, 15041–15055.

33 A. R. Allu, A. Gaddam, S. Ganisetti, S. Balaji, R. Siegel, G. C. Mather, F. Margit, M. J. Pascual, N. Ditaranto, W. Milius, J. Senker, D. A. Agarkov, V. V. Kharton and J. M. F. Ferreira, *J. Phys. Chem. B*, 2018, **122**, 4737–4747.

34 F. Angeli, O. Villain, S. Schuller, S. Ispas and T. Charpentier, *Geochim. Cosmochim. Acta*, 2011, **75**, 2453–2469.

35 F. Muñoz, L. Delevoye, L. Montagne and T. Charpentier, *J. Non-Cryst. Solids*, 2013, **363**, 134–139.

36 F. Angeli, T. Charpentier, E. Molières, A. Soleilhavoup, P. Jollivet and S. Gin, *J. Non-Cryst. Solids*, 2013, **376**, 189–198.

37 S. Plimpton, *J. Comput. Phys.*, 1995, **117**, 1–19.

38 A. Miyake, *Mineral. J.*, 1998, **20**, 189–194.

39 A. Pedone, G. Malavasi, M. C. Menziani, A. N. Cormack and U. Segre, *J. Phys. Chem. B*, 2006, **110**, 11780–11795.

40 P. P. Ewald, *Ann. Phys.*, 1921, **369**, 253–287.

41 S. Nosé, *J. Chem. Phys.*, 1984, **81**, 511–519.

42 W. Shinoda, M. Shiga and M. Mikami, *Phys. Rev. B: Condens. Matter Mater. Phys.*, 2004, **69**, 134103.

43 K. Vollmayr, W. Kob and K. Binder, *Phys. Rev. B: Condens. Matter Mater. Phys.*, 1996, **54**, 15808–15827.

44 A. Stukowski, *Modell. Simul. Mater. Sci. Eng.*, 2010, **18**, 15012.

45 S. Le Roux and V. Petkov, *J. Appl. Crystallogr.*, 2010, **43**, 181–185.

46 E. Sváb, G. Mészáros and F. Deák, *Mater. Sci. Forum*, 1996, **228–231**, 247–252.

47 M. Edén, in *Annual Reports on NMR Spectroscopy*, ed. G. Webb, Academic Press, 2015, vol. 86, pp. 237–331.

48 J. R. Allwardt, S. K. Lee and J. F. Stebbins, *Am. Mineral.*, 2003, **88**, 949–954.

49 A. Pedone, E. Gambuzzi and M. C. Menziani, *J. Phys. Chem. C*, 2012, **116**, 14599–14609.

50 N. K. Nasikas, T. G. Edwards, S. Sen and G. N. Papatheodorou, *J. Phys. Chem. B*, 2012, **116**, 2696–2702.

51 S. K. Lee, G. D. Cody and B. O. Mysen, *Am. Mineral.*, 2005, **90**, 1393–1401.

52 J. F. Stebbins, J. V. Oglesby and S. Kroeker, *Am. Mineral.*, 2001, **86**, 1307–1311.

53 M. Benoit, S. Ispas and M. E. Tuckerman, *Phys. Rev. B: Condens. Matter Mater. Phys.*, 2001, **64**, 224205.

54 P. Ganster, M. Benoit, W. Kob and J.-M. Delaye, *J. Chem. Phys.*, 2004, **120**, 10172–10181.

55 M. Bauchy, *J. Chem. Phys.*, 2014, **141**, 24507.
56 Y. Xiang, J. Du, M. M. Smedskjaer and J. C. Mauro, *J. Chem. Phys.*, 2013, **139**, 44507.
57 S. K. Lee and J. F. Stebbins, *J. Non-Cryst. Solids*, 2000, **270**, 260–264.
58 D. R. Neuville, L. Cormier, V. Montouillout, P. Florian, F. Millot, J. C. Rifflet and D. Massiot, *Am. Mineral.*, 2008, **93**, 1721–1731.
59 C. R. A. Catlow, A. R. George and C. M. Freeman, *Chem. Commun.*, 1996, 1311–1312.
60 J. A. Tossell, *J. Phys. Chem.*, 1996, **100**, 14828–14834.
61 P. J. Dirken, S. C. Kohn, M. E. Smith and E. R. H. van Eck, *Chem. Phys. Lett.*, 1997, **266**, 568–574.
62 A. K. Katz, J. P. Glusker, S. A. Beebe and C. W. Bock, *J. Am. Chem. Soc.*, 1996, **118**, 5752–5763.
63 I. D. Brown, *Chem. Rev.*, 2009, **109**, 6858–6919.
64 R. Oestrike, W.-H. Yang, R. J. Kirkpatrick, R. L. Hervig, A. Navrotsky and B. Montez, *Geochim. Cosmochim. Acta*, 1987, **51**, 2199–2209.
65 S. Iftekhar, B. Pahari, K. Okhotnikov, A. Jaworski, B. Stevensson, J. Grins and M. Edén, *J. Phys. Chem. C*, 2012, **116**, 18394–18406.
66 J. F. Stebbins, E. V. Dubinsky, K. Kanehashi and K. E. Kelsey, *Geochim. Cosmochim. Acta*, 2008, **72**, 910–925.
67 N. Jakse, M. Bouhadja, J. Kozaily, J. W. E. Drewitt, L. Hennet, D. R. Neuville, H. E. Fischer, V. Cristiglio and A. Pasturel, *Appl. Phys. Lett.*, 2012, **101**, 201903.